TRANSIENT ANALYSIS OF HYDRODYNAMIC INTERACTION EFFECTS ON AN AUTONOMOUS UNDERWATER VEHICLE IN PROXIMITY OF A MOVING SUBMARINE

(DOI No: 10.3940/rina.ijme.2015.a4.320)

Z Q Leong, **D Ranmuthugala**, **I Penesis**, and **H D Nguyen,** Australian Maritime College, Tasmania

SUMMARY

When an Autonomous Underwater Vehicle (AUV) is operating close to a moving submarine, the hydrodynamic interaction between the two vehicles can prevent the AUV from maintaining its desired trajectory. This can lead to mission failure and, in extreme cases, collision with the submarine. This paper outlines the transient interaction influence on the hydrodynamic coefficients of an AUV operating in close proximity and in relative motion to a larger moving submarine. The effects of relative motion on the interaction behaviour were investigated via two manoeuvres, i.e. the AUV overtaking and being overtaken by the submarine at different relative forward velocities and lateral distances. The results presented are from a series of Computational Fluid Dynamics (CFD) simulations on axisymmetric AUV and submarine hull forms, with validation of the CFD model carried out through scaled captive model experiments. The results showed that an AUV becomes less susceptible to the interaction influence when overtaking at speeds higher than the submarine. The implications of the interaction influence on the AUV's ability to safely manoeuvre around the submarine are also discussed.

NOMENCLATURE

a_y	Lateral acceleration (m s^{-2})
CB	Centre of buoyancy (m)
C_p	Pressure coefficient; $(p\text{-}p_\infty)/ (0.5\ p_\infty U^2)$
D	Diameter (m)
f	Lateral displacement frequency of the pure sway manoeuvre (s^{-1})
F_I	Inertia force (N)
L	Overall length (m)
L_S	Surface length (m)
m	Mass (kg)
N	Yawing moment (Nm)
N'	Yawing moment coefficient (-); $N/(0.5\rho U^2 L^3)$
$N'_{Interaction}$	Interaction influence on the yawing moment coefficient (-)
p	Pressure (Pa)
p_∞	Freestream pressure (Pa)
Re	Reynolds number (-)
R_{Lat}	Relative lateral distance ratio (-)
R_{Long}	Relative longitudinal distance ratio (-)
R_U	Relative forward velocity ratio (-)
τ	Shear stress (Pa)
u_*	Shear velocity (m s^{-1}); $(\sqrt{\tau/\rho})$
U	Forward velocity of vehicle's centre of buoyancy relative to fluid (m s^{-1})
U_0	Baseline forward velocity (m s^{-1})
Ur	Relative velocity (m s^{-1})
$x_{distance}$	Relative longitudinal distance from the centre of buoyancy (m)
X	Longitudinal force (N)
X'	Longitudinal force coefficient (-); $X/(0.5\rho U^2 L^2)$
$X'_{Interaction}$	Interaction influence on the longitudinal force coefficient (-)
y_a	Lateral displacement amplitude of the pure sway manoeuvre (m)
$y_{distance}$	Relative lateral distance from the centre of buoyancy (m)
Y	Lateral force (N)
Y'	Lateral force coefficient (-); $Y/(0.5\rho U^2 L^2)$
$Y'_{Interaction}$	Interaction influence on the lateral force coefficient (-)
y^+	Non-dimensional wall distance; $(u_* y_{wall})/\nu$
y_{wall}	Mesh node distance to wall (m)
x, y, z	Cartesian coordinates in the x, y, z-direction (m)
ρ	Fluid density (kg m^{-3})
μ	Fluid dynamic viscosity (kg m^{-1} s^{-1})
ν	Fluid kinematic viscosity (m^2 s^{-1}); μ/ρ Volume displacement (m^3)

1. INTRODUCTION

Over the last decade there have been increasing efforts by navies around the world to extend the interoperation capabilities of their submarines with Autonomous Underwater Vehicles (AUVs). This direction in development is driven by the ability of AUVs to operate in hazardous environments for long periods of time with no real-time user intervention, thus mitigating any potential risk away from personnel and high value assets such as submarines and surface ships. These factors are most advantageous for reconnaissance and mine hunting missions. However, for submarine applications such missions often necessitate the AUV and submarine to operate in close proximity in order to launch, recover, and recharge the AUV, in addition to the ability to communicate data between them during operations [5, 11, 21]. This paper focuses on the interaction effects acting an AUV operating close to a moving submarine.

When an AUV is operating in close proximity to a moving submarine (Figure 1), the AUV can experience undesirable changes in its hydrodynamic coefficients due to its interaction with the submarine's wake and pressure fields. These changes can prevent the AUV from maintaining its desired trajectory, which can lead to mission failure and, in extreme cases, collision with the submarine, resulting in damage or destruction of the

AUV and possible damage to the submarine appendages or sensors [4]. Since AUVs are generally much smaller in size relative to submarines, they would be the principle vehicle adversely affected by the interaction. Thus, designers need to have a good understanding of the hydrodynamic interaction between the two vehicles in order to develop adequate and robust AUV control systems to ensure vehicle stability and identify operating parameters in which an AUV can effectively and safely manoeuvre near a moving submarine.

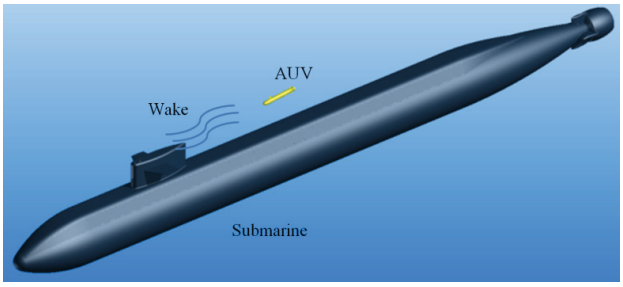

Figure 1: An AUV moving in the wake of a submarine.

For underwater data communication between an AUV and a submarine, acoustic modems can transfer data up to a few kilobits per second over distances well exceeding one thousand meters [9]. Optical modems (i.e. lasers) offer much higher transfer rates of up to a few megabits per second over distances up to a few hundred meters, depending on the turbidity of the water [22]. However, due to the restriction on a submarine to remain covert throughout missions, data transfer with AUVs tends to be carried out at shorter distances or ideally after the recovery of the AUV in order to reduce the probability of detection by third parties. Furthermore, the power source of the AUV is likely to need recharging before progressing to the next mission. This has led to a growing interest in the submarine recovering the AUV for both data transfer and power recharge, thus requiring the AUV to safely negotiate the hydrodynamic interaction effects as it approaches the submarine.

Unlike the recovery of an AUV at the surface, underwater recovery via a submarine presents several unique challenges. Both vehicles rely on their propeller and the hydrodynamic contribution of their control planes for manoeuvring and positioning, thus their hydrodynamic control will reduce as the vehicles reduce speed. Furthermore, unless they have additional side thrusters along their body, they have limited ability to adjust their transverse positions. These factors dictate that the AUV must be recovered while the submarine is moving, with the aid of a mechanism to capture the AUV when it is close enough to the submarine hull in order to overcome the transverse positioning limitations. Further considerations in favour of recovering an AUV via a capture mechanism from a moving submarine are discussed in detail by Irani et al. [12] and Watt et al. [23].

While several studies have focused on recovery options for AUVs via a submarine [4, 11, 12, 23], studies characterising the effects of the hydrodynamic interaction between submerged vessels remain scarce in the public domain. Using steady-state Computational Fluid Dynamics (CFD) simulations, Fedor [7] investigated the hydrodynamic interaction effects on an AUV near a moving submarine with the aim of establishing a feasible region in which to launch and recover the AUV around the submarine sail. It was found that in the forward region of the sail the interaction acts to repel the AUV from the submarine, with the repelling force increasing as the AUV gets closer to the submarine. General trends of the forces and moments acting on the AUV were less observable in the regions to the side and astern of the sail due to disturbances from the horseshoe vortices generated by the sail. The results suggest that it is desirable for recovery to be carried out forward of the sail.

Bryne [3] developed a real-time manoeuvring simulator to evaluate and demonstrate the manoeuvring and control performance of the Phoenix AUV undertaking a docking operation via the torpedo tube of a moving submarine. The hydrodynamic interaction between the two vehicles was modelled by introducing a parabolic flow velocity profile along the submarine hull in order to represent the reduced flow velocity encountered by the AUV as it approached the boundary layer of the submarine. However, this is an over-simplification of the interaction effects, since it did not account for operational issues associated with the more dominant potential field effects generated by a submarine that can either repel or attract the AUV depending on their relative positions.

The studies by Bryne [3] and Fedor [7] offered an insight into the interaction effects acting on an AUV operating within the proximity of a larger moving underwater vessel. However, their investigations focused on locations very close to the submarine, thus the parameters surrounding the broader extent of the interaction effects and the means for the AUV to approach the regions were not discussed.

Rattanasiri et al. [19] used steady-state CFD simulations to investigate the drag force acting on multiple identical ellipsoids representing an AUV fleet in three different formations, i.e. drafting, vee, and echelon. The results showed that the drafting formation reduced the combined drag of the fleet by up to 6% depending on the separation. The vee and echelon formations were found to have limited influence on the combined drag of the fleet, although the leading ellipsoid experienced an increase in drag force while the reverse occurred on the trailing bodies. In their validation test case, a discrepancy of 16% in the drag results was observed between the CFD model predictions and experimental measurements. The discrepancy was attributed to interference drag from the experimental mounting system which was not modelled in the CFD simulations.

The authors have previous published results from CFD and experimental work showing that the behaviour of the interaction depends on the relative size, longitudinal

position, and lateral position between the axisymmetrical hull forms of an AUV and a submarine [17]. The interaction was found to attract and repel the AUV at the stern and bow regions of the submarine respectively. The magnitude of these attraction and repulsion effects varied greatly with only a small change in the relative longitudinal position, suggesting the need for an accurate and fast response control system for the AUV to adequately maintain its trajectory around the moving submarine. However, these adverse interaction effects were found to be minimal around amidships of the submarine, suggesting a safe path for the AUV to approach or depart the submarine laterally within that region. However, the results are from steady-state numerical and experimental work, i.e. the vehicles are travelling forward at the same speed at different fixed relative positions. Therefore, the effects of relative speed between the two vehicles on the interaction effects remain to be established.

This study aims to complement the above work by examining the dynamic effects of the interaction acting on an AUV operating in close proximity and in relative motion to a larger moving submarine. The work was carried out using CFD modelling to quantify the surge force, sway force, and yaw moment acting on the AUV at different speeds, longitudinal positions, and lateral positions relative to the submarine in order to identify the behaviour of the AUV operating in the interaction zone. The CFD predictions were validated and supplemented through experimental captive-model tests. The resulting simulation model is intended to be coupled with a control system in a dynamic manoeuvring simulation to evaluate the motion behaviour of the AUV and develop the necessary algorithms to maintain the desired trajectory of the vehicle when in operation near a moving submarine.

2. INVESTIGATION PROGRAMME

The effects of relative motion on the interaction effects were investigated using two manoeuvres, i.e. the AUV overtaking the submarine and being overtaken by the submarine at different constant relative lateral distances and velocities (Figure 2). The variables investigated included the length-based coefficients of the drag force, sway force, and the yaw moment acting on the AUV, with the latter calculated at a reference point located at the centre of buoyancy of the vehicle. Table 1 summarises the investigation parameters and vehicle dimensions.

The smaller AUV was represented by the axisymmetric SUBOFF hull form [10] developed by the Defence Advanced Research Projects Agency (DARPA), while the larger body representing the submarine was a modified geometry based on the International Submarine Engineer Ltd. designed Explorer [13]. The unappended hull forms of the vehicles (i.e. without sail, control surfaces, and propulsor) enable an unadulterated investigation into the effects of relative size, position, and velocity between the vehicles on the interaction behaviour. The unappended results will be used in further work to identify the effect of vehicle appendages on the interaction behaviour.

Figure 3 shows the two vehicle geometries, with definitions for the principal dimensions, relative longitudinal distance, and relative lateral distance. A diameter ratio (i.e. $D_{\text{Explorer}}/D_{\text{SUBOFF}}$) of 14.634 between the two vehicles was used for the relative motion study as it represents the relative size between a typical AUV and a conventional submarine.

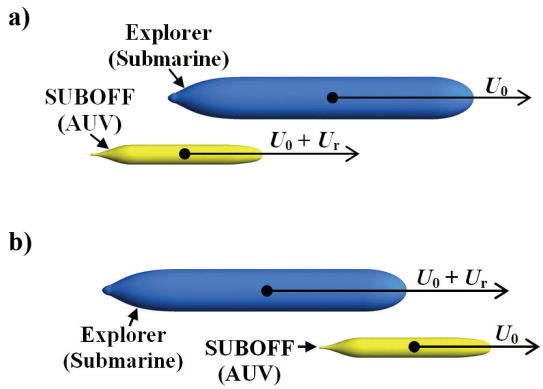

Figure 2: (a) AUV overtaking manoeuvre, (b) and submarine overtaking manoeuvre.

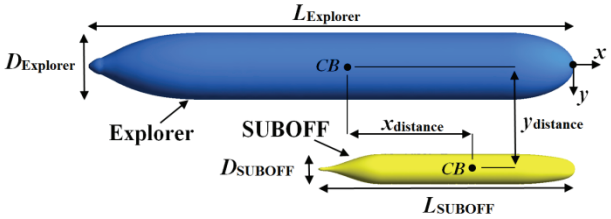

Figure 3: Definition of the model parameters.

The relative lateral distance x_{distance} and relative longitudinal distance y_{distance} were measured from the centre of buoyancy *CB* of the larger vehicle to that of the smaller vehicle. For x_{distance} a 'positive' distance signifies that the SUBOFF is located in front of the *CB* of the larger vehicles. For the remainder of this paper, the longitudinal and lateral distances, and the relative forward and lateral speeds are referred to as non-dimensionalised ratios R_{Long}, R_{Lat}, and R_{U} i.e.,

$$R_{\text{Long}} = \frac{x_{\text{distance}}}{L_{\text{Explorer}}} \quad (1)$$

$$R_{\text{Lat}} = \frac{y_{\text{distance}}}{L_{\text{Explorer}}} \quad (2)$$

$$R_{\text{U}} = \frac{U_0 + U_r}{U_0} \quad (3)$$

Table 1: Vehicle dimensions and investigation parameters.

Parameter	SUBOFF	Explorer	
Length, L	4.570	56.495	[m]
Diameter, D	0.533	7.800	[m]
Displacement, ∇	8.075×10^{-1}	2.309×10^{3}	[m^3]
Base forward speed, U_0	1.50	1.50	[$m\ s^{-1}$]
Longitudinal distance ratio, R_{Long}	-2.00 to 2.00		[-]
Lateral distance ratio, R_{Long}	0.15, 0.21, 0.32, 0.43, 0.71, 1.00		[-]
Relative forward speed ratio, R_U	1.00*, 1.33, 1.67, 2.00, 2.33, 2.67		[-]

*indicates a steady-state approach to the solution

3. SIMULATION SETUP

The simulations were performed using ANSYS CFX 15.0, a commercial CFD code. The Reynolds Averaged Navier-Stokes (RANS)-based Baseline Reynolds Stress Model (BSLRSM) was utilised in this analysis. Previous CFD and Experimental Fluid Dynamics (EFD) work by the authors have established that the BSLRSM was more accurate in predicting the forces and moments acting on underwater vessels of similar geometry to the SUBOFF, compared to the RANS-based eddy-viscosity models within CFX [16]. This is due to the BSLRSM's more comprehensive modelling of rotational flow, flow separation, and flows that are strongly anisotropic.

For the transient simulations, the ANSYS Meshing Platform (AMP) re-meshing method was used to simulate the relative motion between the two bodies. This enabled the investigation of the effects of relative speed on the interaction behaviour between the two bodies which is not achievable via steady-state simulations. The essential characteristic of this method is that the mesh in the fluid domain deforms locally around the object as it moves, and re-meshes when the mesh quality is deemed compromised in terms of accuracy and stability. This overcomes the limited motions imposed by using a pure mesh deformation approach, and allows adequate modelling of the boundary layer and rotation of the bodies compared to other dynamic mesh methods within CFX, as discussed by the authors in et al. [15].

Figure 4 shows the computational fluid domain in a fixed frame of reference, with its centre of origin located at the centre of buoyancy of the Explorer ($CB_{Explorer}$). The far field boundaries were kept six body lengths away from the $CB_{Explorer}$, with the exception of the outlet, which was kept eight body lengths away. This ensured that boundaries had no blockage effect on flow around the vehicle geometries, and that the wake due to each vehicle was sufficiently resolved within the domain. The flow at the inlet was prescribed to match the desired vehicle speed, while the outlet was set as an opening with zero relative pressure. The surfaces of the vehicles were prescribed as no-slip walls, while the remaining boundaries were set as free-slip walls.

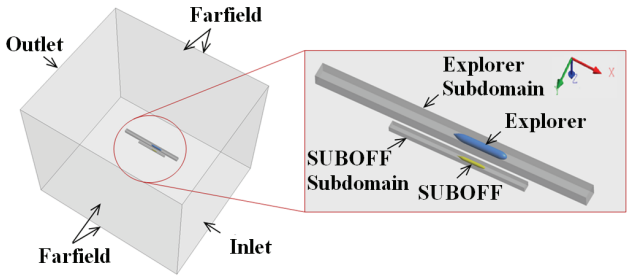

Figure 4: Computational fluid domain.

The fluid domain was divided into three parts: two subdomains for each of the regions around the Explorer and SUBOFF, and an outer domain for the remaining region. The division of the domain allowed the mesh of the vehicle sub-domains to be kept rigid during the solver process, while the outer domain underwent mesh deformation and re-meshing, thus maintaining mesh quality around the vehicles and reducing the re-meshing time. For the discretisation of the fluid domain, an unstructured mesh approach was used, i.e. triangular prismatic inflation layers around the SUBOFF to capture the boundary layer and unstructured tetrahedrons in the far field. The unstructured mesh approach was selected due to its ability to easily accommodate the mesh deformation and re-meshing. The unstructured mesh approach, although it requires a higher mesh density, has also been proven to offer the same degree of accuracy in comparison to a structured mesh [6]. The "high resolution" advection scheme was used for the simulations. This is the most comprehensive advection scheme available within ANSYS CFX [1].

4. EXPERIMENTAL WORK

In order to supplement and establish the credibility of the CFD predictions, a series of captive-model experiments were conducted in the Australian Maritime College (AMC) Towing Tank. The experiments involved two testing regimes: transient measurements of the SUBOFF undergoing a pure sway manoeuvre, i.e. $y_a\sin(2\pi f)$, adjacent to the Explorer while maintaining a constant R_{Long} (Figure 5), and steady-state measurements of the SUBOFF fixed at different R_{Long} to the Explorer while maintaining a constant R_{Lat} (i.e. $y_a = 0$). For both manoeuvres, the two vehicles were travelling at the same constant forward speed. The experimental parameters of the manoeuvres are outlined in Table 2.

The pure sway manoeuvre has been selected for this study as it provides a good assessment of the CFD model's ability to predict the transient forces and moments associated with the accelerative motions of the manoeuvre. The pure sway manoeuvre is also widely used by other researchers in numerical and experimental studies [2, 8, 18] to characterise the hydrodynamic derivatives of underwater vehicles.

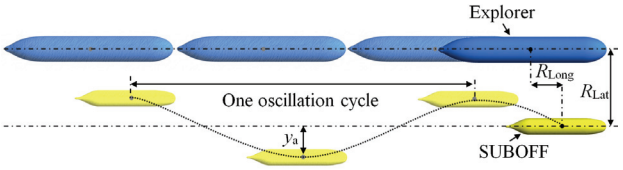

Figure 5: SUBOFF undergoing a pure sway manoeuvre at a constant R_{Long} to the Explorer.

Table 2: Experimental parameters.

Parameter	SUBOFF	Explorer	Unit
Length, L	1.552	2.935	[m]
Diameter, D	0.181	0.405	[m]
Displacement, ∇	3.162×10^{-2}	3.237×10^{-1}	[m^3]
Overtaking manoeuvre (steady-state)			
Longitudinal distance ratio, R_{Long}	-0.62 to 0.92	-	[-]
Lateral distance ratio, R_{Lat}	0.21	-	[-]
Base forward speed, U_0	1.50	1.50	[-]
Reynolds Number, Re	2.61×10^{6}	4.93×10^{6}	[-]
Pure sway manoeuvre (transient)			
Longitudinal distance ratio, R_{Long}	0.23	-	[-]
Lateral distance ratio, R_{Lat}	0.21	-	[-]
Base forward speed, U_0	1.20	1.20	[m s^{-1}]
Reynolds Number, Re	2.09×10^{6}	3.95×10^{6}	[-]
Sway oscillation frequency, f	0.2	-	[Hz]
Sway amplitude, y_a	0.14	-	[m]

The 100m×3.5m×1.5m tank is equipped with a manned variable speed carriage and a wave generator, and uses a Horizontal Planar Motion Mechanism (HPMM) capable of generating horizontal motion on the underwater vehicle model, and recording the resulting forces and moments. The SUBOFF model was mounted to the HPMM using a 'sting' arrangement that connects to the model through the aft end, with the forces acting on the SUBOFF model recorded via two 6-Degree of Freedom (6-DOF) load cells located inside the model as shown in Figure 6. The Explorer model was mounted directly onto the carriage by means of rigid supports as shown in Figure 7, with no forces recorded, as the objective of the work was to investigate the behaviour of the smaller vehicle due to the interaction.

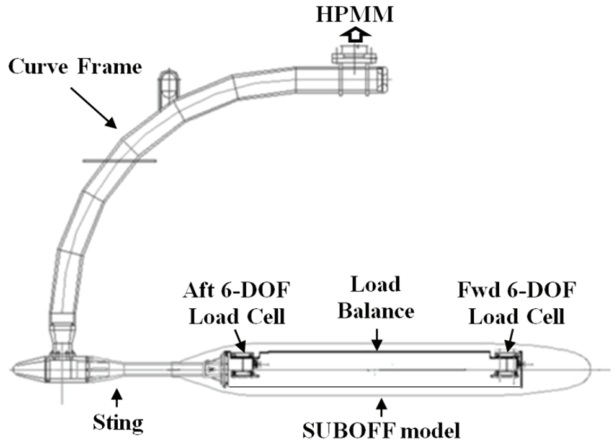

Figure 6: SUBOFF support rig.

The R_{Lat} between the two models was adjusted by shifting the lateral position of the SUBOFF using the HPMM, while the R_{Long} was adjusted by shifting the longitudinal position of the Explorer along the support beam. Both models were fully flooded and located at mid-depth of the tank.

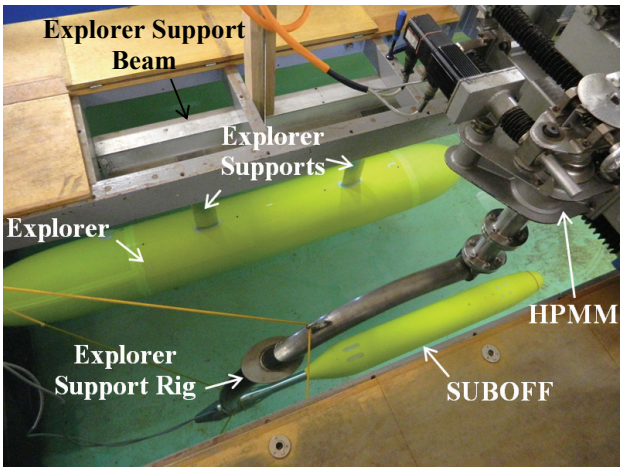

Figure 7: Experimental testing rig.

5. CFD VERIFICATION AND VALIDATION

5.1 MESH INDEPENDENCE STUDY

In order to establish the mesh requirements for the simulations, the effects of the mesh resolution on the predicted interaction forces and moments acting on the SUBOFF model were examined. The mesh study was conducted at a speed of $Re_{Explorer} = 9.545\times10^{7}$, with the SUBOFF fixed at R_{Long} and R_{Lat} of 0.00 and 0.21 respectively. The surface mesh size on the SUBOFF and Explorer was selected as the refinement variable for the mesh study.

An initial mesh model was created based on the following criteria: a maximum Curvature Normal Angle of 9° (which creates 10 circumferential divisions along a 90° circular arc) in order to provide adequate resolution of the vehicles' curvature and a maximum domain mesh body size equivalent to the diameter of the Explorer. The non-dimensional distance (y^+) of the first inflation layer around the SUBOFF and Explorer for the various simulation runs was maintained below one in order to adequately resolve the boundary layer and accurately predict the off-axis hydrodynamic forces and moments on the vehicles using the BSLRSM simulation [16]. In order to account for the effects of the vehicle's curvature on the boundary layer thickness, the total thickness of the inflation layers around the vehicles was matched to two times Prandtl's theoretical estimate of turbulent boundary layer thickness over a flat plate, i.e. $2\times0.16L_S/Re_{L_S}^{1/7}$, where L_S is the surface length of the vehicle. The authors have found from previous CFD work [16] that underprescribing the total thickness of the inflation layers below 1.5 times the theoretical estimate results in higher longitudinal force predictions and lower lateral force predictions. Over-prescribing the total thickness of the inflation layers has no noticeable effect on the predictions.

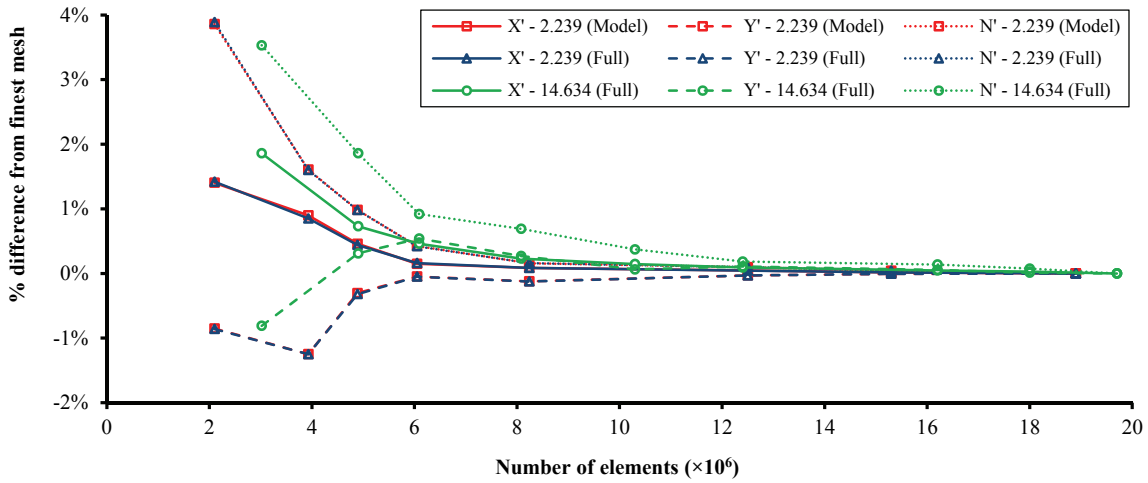

Figure 8: Percentage difference of the longitudinal force coefficient *X'*, lateral force coefficient *Y'*, and yawing moment coefficient *N'* predictions against the finest mesh solution as a function of number of mesh elements for the model scale and full scale diameter ratios investigated.

Figure 8 shows the percentage difference of the predicted longitudinal force, lateral force, and yawing moment for the finest mesh solution as a function of mesh element density for the diameter ratios investigated. For the 2.239 diameter ratio, it is seen that at 3.9 million elements and above, the forces and moment predictions for both the model scale and full scale were within 2% of the finest mesh investigated. For the diameter ratio of 14.634, the forces and moment predictions were within 2% of the finest mesh investigated at around 4.9 million elements. The increase in mesh density requirement for mesh independence as the diameter ratio increases is due to the decrease in the displacement of the SUBOFF. As a conservative measure the 4.9 and 6.0 million elements mesh model configurations were used to represent the 2.239 and 14.634 diameter ratio simulations respectively, as they were well within 1% of the forces and moment predictions of the finest mesh investigated and thus deemed to provide a mesh independent solution.

5.2 VALIDATION AGAINST EXPERIMENTS

In order to assist with the validation, the CFD model was made to replicate the experimental setup. The free surface of the water and the experimental rig used to support the vehicles were included in the simulation model (Figure 9) in order to account for their effects on the interaction forces and moments acting on the SUBOFF. The computational fluid domain was given the same dimensions as the AMC towing tank except for the domain length, which was reduced from 100m to 40m in order to reduce the computational requirement while ensuring that the pressure and wake fields generated by the vehicles were well resolved within the numerical domain.

To account for the inertia forces associated with the accelerative motions in the pure sway manoeuvre, the water entrained within the SUBOFF model was also modelled (Figure 10). The inertia contribution of the SUBOFF shell and mounting was modelled based on Newton's second law of motion, i.e. $F=ma_y$, where F is the inertia force, m is the mass (7.4kg), and a_y is the acceleration of the sway motion

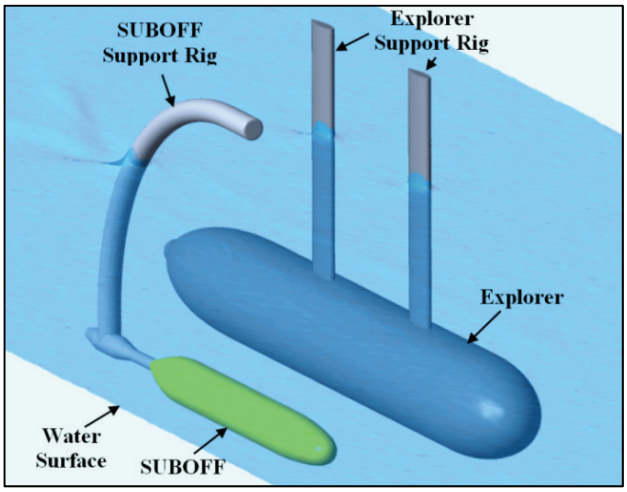

Figure 9: CFD model of the experimental setup, including the free surface and support rigs.

5.2 (a) Overtaking Manoeuvre (Steady-State)

Figure 11 shows the CFD predicted longitudinal force, lateral force, and yawing moment coefficients acting on the SUBOFF at different R_{Long} in comparison with the experimental measurements for the diameter ratio of 2.239 at model scale. The figures show good agreement between the CFD and experimental results throughout the R_{Long} range, with the difference being less than the experimental uncertainty as determined using the recommended analysis procedure outlined in ITTC [14], i.e. 2.252×10^{-4} for the force coefficients and 1.446×10^{-4} for the moment coefficients.

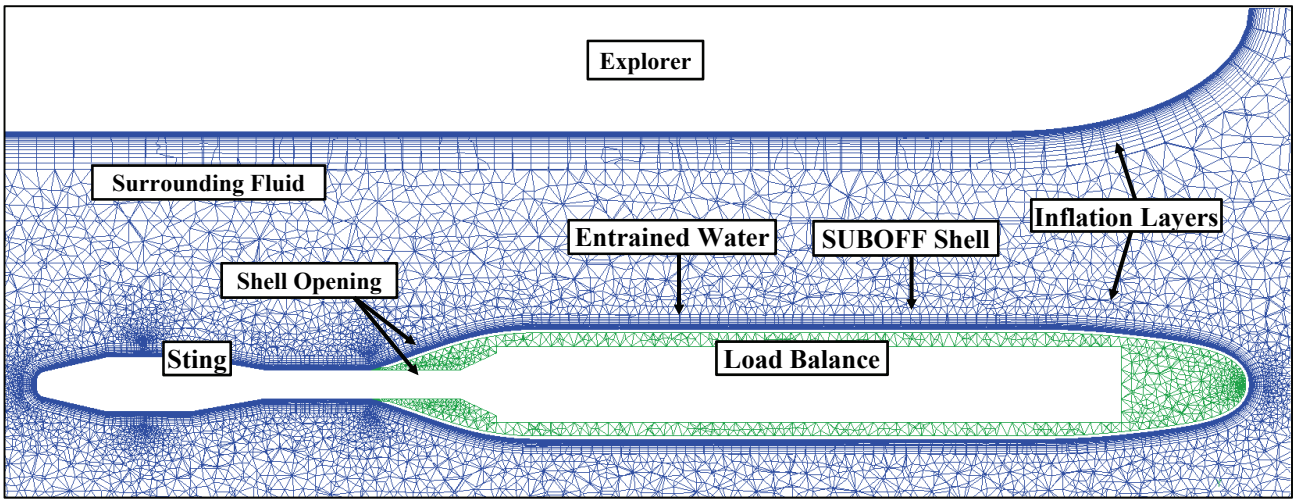

Figure 10: Mesh model of the experimental setup with the entrained water within the SUBOFF shell modelled to account for its inertia effects.

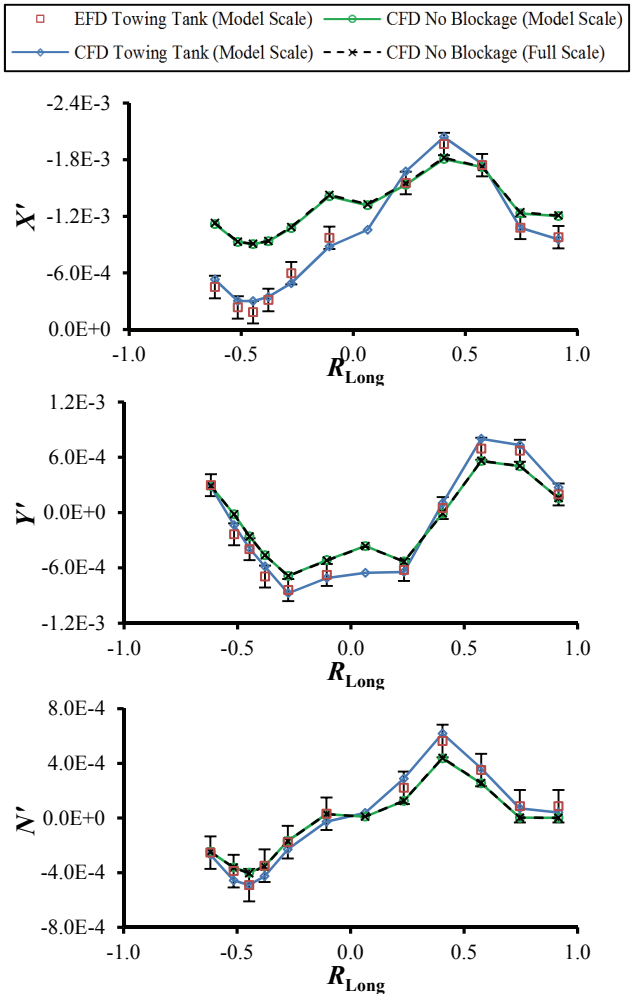

Figure 11: CFD and experimental results of the longitudinal force coefficient *X'* (top), lateral force coefficient *Y'* (middle), and yawing moment coefficient *N'* (bottom) on the SUBOFF as a function of longitudinal separation ratio R_{Long} for the diameter ratio of 2.239 at $Re_{SUBOFF} = 2.61\times10^6$, $Re_{Explorer} = 4.93\times10^6$, and $R_{Lat} = 1.70$. The error bars indicate the experimental uncertainty, i.e. 2.252×10^{-4} for the force coefficients and 1.446×10^{-4} for the moment coefficients.

Figure 11 also shows the CFD model scale and full scale predictions with and without towing blockage and free surface effects on the flow around the vehicles. The latter was achieved by extending the domain boundaries six $L_{Explorer}$ away from the $CB_{Explorer}$, with the exception of the outlet which was kept eight body lengths away. The model scale predictions with the extended boundaries indicated substantial blockage effect in the EFD measurements, particularly in the longitudinal force coefficient when the SUBOFF was located at the stern region of the Explorer, i.e. $R_{Long}<0.00$. Thus, the extended domain was used for the remainder of the study, with the reduced domain used only for validation purposes. The model scale and full scale predictions with the extended boundaries were found to be in close agreement, demonstrating that the Re scaling based on the $L_{Explorer}$ was appropriate for maintaining dynamic similarity between the two scales and thus providing sufficient validation for the CFD model to be extended to the full scale cases investigated.

5.2 (b) Pure Sway Manoeuvre

Figure 12 shows the CFD predicted longitudinal and lateral force coefficients acting on the SUBOFF as a function of time in comparison with the experimental measurements for the pure sway manoeuvre test case obtained using the HPMM. The figure shows good agreement between the CFD and experimental results, with the differences well within the experimental force and moment coefficient uncertainty, and time and phase differences of less than 0.1s and 8° respectively. The Courant Number was maintained below 20 for transient simulations given that ANSYS CFX is an implicit solver. Thus, a higher priority was given towards the time step sensitivity of the simulation predictions. The time step used for the CFD simulation was 0.02s as the phase and magnitude of the predictions were found to be well within a 1% error margin of the predictions using a time step of 0.005s.

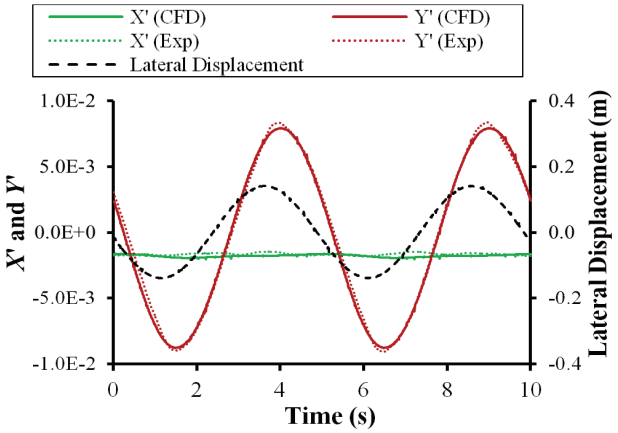

Figure 12: CFD and experimental time traces of the longitudinal force coefficient *X'* and lateral force coefficient *Y'* on the SUBOFF for the 0.2Hz pure sway manoeuvre; $Re_{SUBOFF} = 2.09\times10^6$, $Re_{Explorer} = 3.95\times10^6$, and diameter ratio = 2.239.

6. RESULTS AND DISCUSSION

The following discussion focuses on the influence of the interaction on the SUBOFF's hydrodynamic coefficients for the following two manoeuvres: SUBOFF overtaking the Explorer, and SUBOFF overtaken by the Explorer. The magnitudes of the interaction influence were obtained by subtracting the baseline SUBOFF's hydrodynamic coefficients (at R_{Long} = -2.0) from the results for the range of parameters outlined in Table 1. The results are presented as a function of the relative longitudinal position between the two vehicles.

6.1 AUV OVERTAKING MANOEUVRE

6.1 (a) Effect of relative longitudinal position

Figure 13 shows the interaction influence on the longitudinal force, lateral force, and yawing moment coefficients of the SUBOFF as it overtakes the Explorer at a constant R_{Lat} of 0.21. As the SUBOFF approaches the Explorer, the stern pressure field of the latter acts to reduce the SUBOFF's longitudinal force coefficient, laterally attracts the SUBOFF, and yaws the SUBOFF bow towards the Explorer. The influence of these interaction effects increases as the SUBOFF progresses forward and peaks at around R_{Long} of -0.4. Thus, the stern region of the submarine presents a high risk of collision for an AUV to operate within, for an AUV maintaining a straight-line overtaking trajectory with no additional control under the influence of the interaction. In the event of collision it is possible for the AUV to lose forward speed and be drawn into the submarine's propeller. The combination of these adverse effects and implications makes it undesirable for an AUV to approach the submarine from the stern.

As the SUBOFF progresses onwards from R_{Long} of -0.4, the interaction influence declines and recovers to the base value at around R_{Long} of 0.0. At R_{Long} of 0.2 onwards, the forward pressure field of the Explorer acts to increase the SUBOFF's longitudinal force coefficient, laterally repel the SUBOFF, and yaw the SUBOFF bow away from the Explorer. The influence of these interaction effects peaks at around R_{Long} of 0.4, and then declines and diminishes at around R_{Long} of 1.5 as the SUBOFF clears away from the pressure field of the Explorer. The trends suggest that an AUV will encounter difficultly in approaching the bow of the submarine as the influence of the interaction acts to repel the AUV as it passes within that region. The interaction influence was found to be minimal around the amidships of the submarine, where its negative pressure field is fairly uniform (see Figure 14), thus suggesting a safe region for the AUV to manoeuvre within.

6.1 (b) Effect of relative speed

Five overtaking velocities were evaluated and compared with the steady-state results at a constant R_{Lat} of 0.21 (see Figure 13). The magnitude of the interaction influence reduces as the SUBOFF overtakes at higher relative velocities to the Explorer. This is due to an increase in the SUBOFF pressure field intensity at higher overtaking speeds, thus reducing the pressure difference between the SUBOFF and the Explorer. This suggests that an AUV becomes less susceptible to the interaction influence when overtaking at speeds higher than the submarine. The general trends of interaction influence with respect to R_{Long} at the different overtaking speeds were similar to the findings discussed in Section 6.1(a).

Since an AUV relies on its control planes and propeller for trajectory control, the hydrodynamic coefficients of the fully appended SUBOFF (see Roddy [20]) is used as an indication of the ability of an AUV to effectively manoeuvre under the influence of the interaction. The following discussion is based on the SUBOFF's yawing moment coefficient, as this determines the tendency of the vehicle to adjust its angle of attack given known control forces. The resultant change in angle of attack then acts to generate the directional thrust and lateral forces required to effectively manoeuvre.

From Figure 13, the interaction influence on the SUBOFF yawing moment coefficients in positive and negative directions were found to be at their highest when the SUBOFF maintains its position (U_R = 0 m/s) at R_{Lat} of -0.4 and 0.4; i.e. $N'_{Interaction}$ of -3.3 x 10^{-4} and 3.7 x 10^{-4} respectively. Based on the SUBOFF's hydrodynamic coefficients measured by Roddy [20], the $N'_{Interaction}$ values are within the maximum yawing moment contribution of the SUBOFF stern rudders (which is approximately 7.0 x 10^{-4} at the maximum rudder angle of 15 degrees). However, the manoeuvrability of the SUBOFF will be extremely limited at these points considering that the maximum angle of attack that can be maintain by the SUBOFF is 2 degrees bow towards and away from the Explorer at R_{Lat} of -0.4 and 0.4

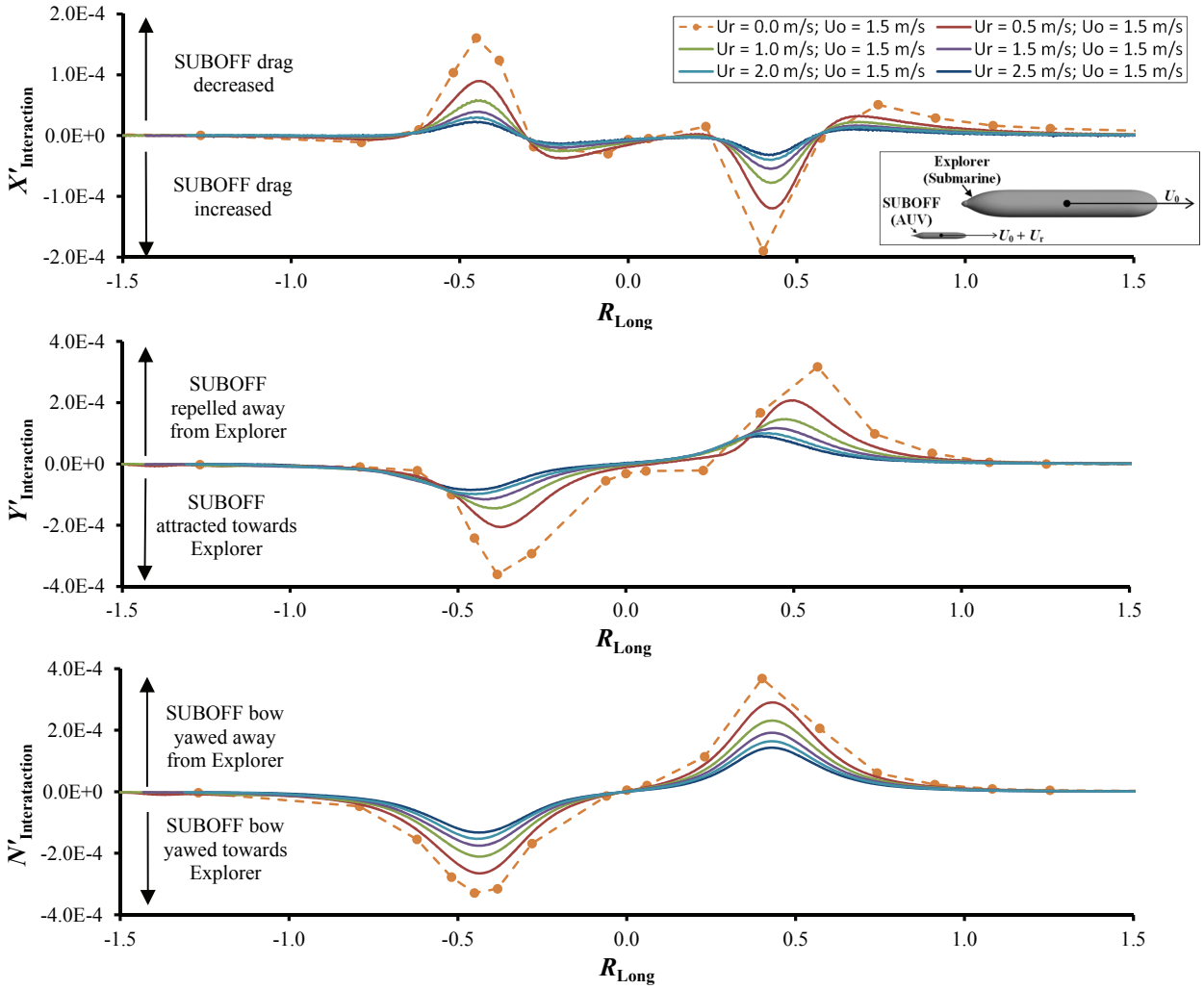

Figure 13: Interaction influence on the SUBOFF's longitudinal force coefficient ($X'_{\text{Interaction}}$), lateral force coefficient ($Y'_{\text{Interaction}}$), and yawing moment coefficients ($N'_{\text{Interaction}}$) vs relative longitudinal position (R_{Long}) for the AUV overtaking the submarine at different relative speeds.

respectively. Above these thresholds, the SUBOFF bow will be increasingly yawed towards the Explorer at the R_{Lat} of -0.4 and in the opposite direction at the R_{Lat} of 0.4 due to the combination of the interaction influence and the hydrodynamic contribution of the SUBOFF barehull. This suggests that it is unlikely for an AUV to safely negotiate the interaction effects around the stern and bow regions of a moving submarine, especially in the case of a recovery operation within these regions.

Figure 15 gives the interaction influence on the longitudinal force, lateral force, and yawing moment coefficients of the SUBOFF as it overtakes the Explorer at different R_{Lat}. The forward speeds of the SUBOFF and Explorer are 3.0 m/s and 1.5 m/s respectively (i.e. U_0 = 1.5 m/s, U_r = 1.5 m/s).

The interaction influence on the SUBOFF's hydrodynamic coefficients were found to be negligible at R_{Lat} of 1.00, with magnitudes less than 1 x 10^{-5}. As the lateral distance between the vehicles decreased, the interaction influence gradually increased, with the trends against R_{Long} similar to those discussed in Section 6.1(a). The exception are that the peak and trough of the interaction influence on the SUBOFF's longitudinal force coefficients become more prominent between the R_{Long} of -0.3 and 0.3, as the R_{Lat} reduced from 0.21 to 0.15 (which is approximately 8.0m and 4.5m away from the Explorer hull, respectively). Figure 14 shows that the positive and negative pressure fields of the Explorer propagating from the stern and bow, thus the pressure gradient in which the SUBOFF manoeuvres is much greater longitudinally at R_{Lat} of 0.15 alongside the Explorer. Therefore, it is desirable that the recovery operation of an AUV via a capture mechanism to be designed with these changes in mind, either by extending the capture mechanism outside the region adversely affected by the longitudinal force changes, or an AUV control system that is capable of responding sufficiently quickly to the changes in its longitudinal force coefficient in order to maintain its relative position.

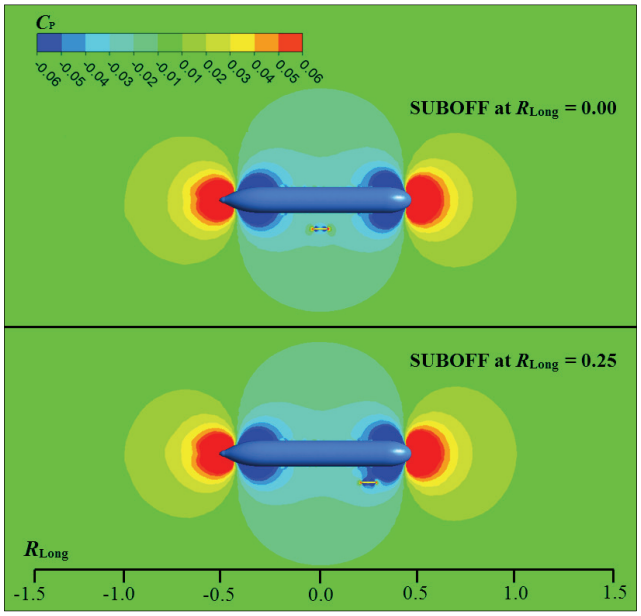

Figure 14: Pressure coefficient (C_P) contours of the flow around the SUBOFF and Explorer models at R_{Long} = 0.00 (top) and R_{Long} = 0.25 (bottom); R_{Lat} = 0.15. The pressure coefficient contour range is clipped at ±0.06.

6.1 (c) Effect of lateral distance

Further examination of Figure 15 revealed that the increase in the interaction influence on the SUBOFF's lateral force and yawing moment coefficients as R_{Lat} is decreased can be idealised by empirical equations obtained through power regression analysis of the data (see Figure 16). However, the general trend of interaction influence on the SUBOFF's drag coefficient as a function of both R_{Lat} and R_{Long} (as discussed earlier) was less observable, thus necessitating that the evaluation of close proximity manoeuvres of such vehicles be carried out through virtual, experimental, or real world testing rather than through empirical models in order to realistically represent the nature of such operations.

6.2 SUBMARINE OVERTAKING MANOEUVRE

6.2 (a) Effect of relative longitudinal position

Figure 17 shows the interaction influence on the longitudinal force, lateral force, and yawing moment coefficients of the SUBOFF as it overtaken by the Explorer at a constant R_{Lat} of 0.21.

As the Explorer approaches the SUBOFF, the interaction influence on the latter is observable at around R_{Long} of 1.6, as it enters the positive bow pressure field of the Explorer resulting in a decrease in its drag coefficient (see Figure 14). At around R_{Long} of 0.6, the interaction acts to increase the SUBOFF drag. This is due the negative pressure field around the bow region of the Explorer progressing onto the SUBOFF's stern, while the bow of the latter remains in the positive pressure field. The increase in drag peaks at around R_{Long} of 0.4, and then declines and recovers to the base value at around R_{Long} of 0.3. Between the R_{Long} 0.3 and 0.0, the SUBOFF experiences a drag reduction due its stern moving into a relatively higher pressure field. At R_{Long} of 0.0, the Explorer pressure field in which the SUBOFF resides is relatively uniform longitudinally and thus the interaction has a minimal effect on the SUBOFF drag. As the Explorer progresses forward, the SUBOFF experiences an increase in drag up to R_{Long} of -0.3, from which point onwards the interaction influence acts to reduce the SUBOFF drag. The drag reduction reaches its maximum value at around R_{Long} of 0.4 and then declines. At R_{Long} of -0.6 onwards the SUBOFF begins to experience an increase in drag which gradually recovers to the base value at an R_{Long} of -1.3 as the Explorer's pressure field clears away from the SUBOFF.

With regards to the interaction influence on the lateral coefficient, the Explorer acts to repel the SUBOFF as it approaches at around R_{Long} of 1.3. The repulsion increases to its maximum value at around R_{Long} of 0.6, before steeply declining to the base value at around R_{Long} of 0.5. Between R_{Long} of 0.5 and -0.5, the interaction acts to attract the SUBOFF. Two prominent troughs of the attraction occur at 0.3 and -0.3. As the Explorer progresses from R_{Long} of 0.4, the interaction acts to repel the SUBOFF from the Explorer, increasing to its maximum value at around R_{Long} of -0.6 and then declines to a negligible magnitude at around R_{Long} of 1.3.

The trend of the interaction influence on the SUBOFF's yawing moment coefficient was found to be similar to that for the AUV overtaking the submarine (see Section 6.1), with the Explorer acting to yaw the SUBOFF bow away and towards the former at the Explorer bow and stern regions respectively.

6.2(b) Effect of relative velocity

The interaction influence on the SUBOFF's hydrodynamic coefficients when overtaken by the Explorer at five different relative velocities were evaluated and compared with the steady-state results at a constant R_{Lat} of 0.21 (see Figure 17).

The magnitude of the interaction influences is shown to increase as the Explorer overtakes at higher relative velocities to the SUBOFF. While the general trends of the interaction influence were similar to the AUV overtaking the submarine (see Section 6.1), the magnitudes of interaction influence for the submarine overtaking the AUV were much more pronounced. These magnitudes were much more than the steady-state results and exceeded the hydrodynamic contribution of the SUBOFF control planes significantly. This suggests that it is unlikely that an AUV will be able to negotiate the interaction influence or maintain its trajectory when overtaken by a submarine at close proximity without larger control planes, which in turn may create additional interaction issues.

7. CONCLUSION

The paper presents a study conducted to quantify the behaviour of an AUV operating in close proximity to a larger moving submarine at different relative velocities. The investigation utilised CFD and EFD techniques to quantify the longitudinal force, lateral force, and yawing moment coefficients of the AUV with respect to the different relative longitudinal positions between the two vehicles in order to characterise the behaviour of the AUV under the influence of the interaction.

The EFD results from captive model tests were used to validate the CFD model and showed good agreement, thus enabling the latter to be used for further analysis of the interaction under full scale conditions. The effects of relative velocities on the interaction behaviour were investigated via two manoeuvres: the AUV overtaking the submarine and vice versa, both at a constant relative lateral distance. The effects of lateral distance (R_{Lat}) on the interaction were also investigated for the AUV overtaking the submarine.

The results showed that an AUV becomes less susceptible to the interaction influence when overtaking at speeds higher than the submarine. The general trend of the results showed that the submarine's stern presents a high collision risk region for an AUV to travel within, as the interaction forces and moments tend to attract the AUV towards the submarine. Similarly, the bow region of the submarine is difficult for an AUV to approach as the interaction forces and moments act to repel the AUV away from the submarine. The adverse interaction effects were found to be minimal around amidships of the submarine throughout the different relative velocities examined, suggesting a safe path for the AUV to approach or depart the submarine laterally around this region.

The interaction influence of the submarine's bow and stern regions on the AUV's lateral force and yawing moment coefficients were found to vary as a power of R_{Lat}, with the two coefficients increasing as the R_{Lat} decreases. General trends of the effects of R_{Lat} on the interaction influence on the AUV's longitudinal force coefficient as a function of R_{Long} were less observable. Therefore, it is desirable that the evaluation of manoeuvres involving close proximity between an AUV and a submarine to be carried out through virtual, experimental, or real world testing of the vehicles rather than through empirical models in order to realistically represent the behaviour of the vehicles.

In the case of the submarine overtaking the AUV, the interaction influence on the latter's hydrodynamic coefficients were found to exceed the ability of the AUV's control planes to compensate. Therefore, it is unlikely that an AUV will be able to maintain its trajectory when approached by a submarine with sufficiently large control planes. However, larger control planes may cause additional interaction affects.

Further work is being undertaken to extend the current assessment of the interaction behaviour for fully appended models of the AUV and the submarine, in order to identify the interaction influence of the vehicles' appendages (i.e. sail and control planes) and propeller. The addition of the appendages and propellers are expected to amplify the interaction effects on the AUV's hydrodynamic coefficients. These fully appended vehicle models are intended to be used in a dynamic manoeuvring simulation to evaluate the operating parameters in which an AUV can safely approach a submarine for recovery, and develop the necessary control algorithms for the AUV to successfully negotiate the manoeuvres.

8. REFERENCES

1. ANSYS, Advection Scheme Selection, *CFX-Solver Modelling Guide – Release 15.0,* ANSYS, Inc., 2014.
2. AZARSINA, F., WILLIAMS, C.D., and ISSAC, M.T., Modelling the Hydrodynamic Sway Force Exerted on the Bare-Hull of an Axi-sysmmetric Underwater Vehicle in Lateral Acceleration Manoeuvres, *Proceedings of Oceans 2008*, 2008.
3. BRYNE, K.M., *Real-Time Modelling of Cross-Body Flow for Torpedo Tube Recovery of The Phoenix Autonomous Underwater Vehicle (AUV)*, Naval Postgraduate School, California, USA, 1998.
4. CURRIE, J., GILLIS, C.B., CARRETERO, J.A., DUBAY, R., JEANS, T., WATT, G.D., Dynamics of Two Active Autonomous Dock Mechanisms for AUV Recovery, *Transactions of the Canadian Society for Mechanical Engineering*, 2014.
5. DARPA, *Hydra Proposers' Day*, Defense Advanced Research Projects Agency, Virginia, USA, 2013.
6. DUDA, B.M., MENTER, F.R., HANSEN, T., AND ESTEVE, M-J., Scale-adaptive simulation of a hot jet in cross flow, *Journal of Physics: Conference Series*, *Volume 318, pp 1-6*, 2011.
7. FEDOR, R., *Simulation of a Launch and Recovery of an UUV to a Submarine*, Royal Institute of Technology, Sweden, 2009.
8. GRANLUND, K., *Steady and Unsteady Maneuvering Forces and Moments on Slender Bodies*, Virginia Polytechnic Institute and State University, USA, 2009
9. GALLIMORE, E., PARTAN, J., VAUGHN, I., SINGH, S., SHUSTA, J., AND FREITAG, L., *The WHOI Micromodem-2: A Scalable System for Acoustic Communications and Networking*, IEEE Oceans Conference, Seattle, 2010.

10. GROVES, N., HUANG, T., AND CHANG, M., *Geometric Characteristics of DARPA SUBOFF Models (DTRC Models Nos. 5470 and 5471)*, David Taylor Research Center, Maryland, 1989.
11. HARDY, T., BARLOW, G., Unmanned Underwater Vehicle (UUV) deployment and retrieval considerations for submarines, *Proceedings of the 11th International Naval Engineering Conference*, Hamburg, Germany, 2008.
12. IRANI, R.A., KEHOE, D., SPENCER, W.W., WATT, G.D., GILLIS, C., CARRETERO, J.A., AND DUBAY, R., Towards a UUV and Recovery System on a Slowly Moving Submarine, *Warship 2014: Naval Submairnes & UUV*, *Bath, UK*, 2014.
13. ISE, *Explorer Autonomous Underwater Vehicle Datasheet*, International Submarine Engineering Ltd., Canada, 2005.
14. ITTC, Recommended Procedures and Guidelines: Testing and Extrapolation Methods: Resistance- Uncertainty Analysis, Example for Resistance Test, *ITTC Recommended Procedures and Guidelines*, *Procedure 7.5-02-02-02*, 2002.
15. LEONG, Z.Q., RANMUTHUGALA, D., PENESIS, I., AND NGUYEN, H., Numerical Simulation of Spheres in Relative Motion Using Dynamic Meshing Techniques, *Proceedings of the 18th Australasian Fluid Mechanics Conference*, Launceston, Australia, 2012.
16. LEONG, Z.Q., RANMUTHUGALA, D., PENESIS, I., AND NGUYEN, H., RANS-based CFD Prediction of the Hydrodynamic Coefficients of DARPA SUBOFF Geometry in Straight-Line and Rotating Arm Manoeuvres, *International Journal of Maritime Engineering*, 157, 41-52, 2015.
17. LEONG, Z.Q., RANMUTHUGALA, D., PENESIS, I., AND NGUYEN, H., Scaling and Relative Size Effects on the Hydrodynamic Interaction on an UUV operating close to a Submarine, *Proceedings of Warship 2014: Naval Submarines and UUVs*, *Bath, UK*, 2014.
18. PHILLIPS, A.B., FURLONG, M., AND TURNOCK, S.R., Virtual planar motion mechanism tests of the autonomous underwater vehicle Autosub, *STG-Conference/ Lecture day "CFD in Ship Design",* Hamburg University of Technology, 2007
19. RATTANASIRI, P., WILSON, P.A., AND PHILLIPS, A.B., Numerical investigation of a fleet of towed AUVs, Ocean Engineering, 80, 25-35, 2014.
20. RODDY, R.F., *Investigation of the Stability and Control Characteristics of Several Configurations of the DARPA SUBOFF Model (DTRC Model 5470) from Captive-Model Experiments*, David Taylor Research Center, Maryland, 1990.
21. RODGERS, J., WHARINGTON, J., TYNAN, A., AND COXHEAD, M., A concept for the deployment of unmanned maritime systems from submarines: MURULA integration, impact modelling and results, *Proceedings of the Undersea Defence Technology Conference, Sydney, Australia*, 2008.
22. SCHOLZ, T., 'Using Laser Communication Above Water and Underwater', *Sea Technology*, Compass Publications Inc., 2011.
23. WATT, G.D., CARRETERO, J.A., DUBAY, R., MACKENZIE, M.R., Towards an Automated Active UUV Dock on a Slowly Moving Submarine, *Proceedings of Warship 2011: Naval Submarines and UUVs*, *Bath*, *UK,* 2011.

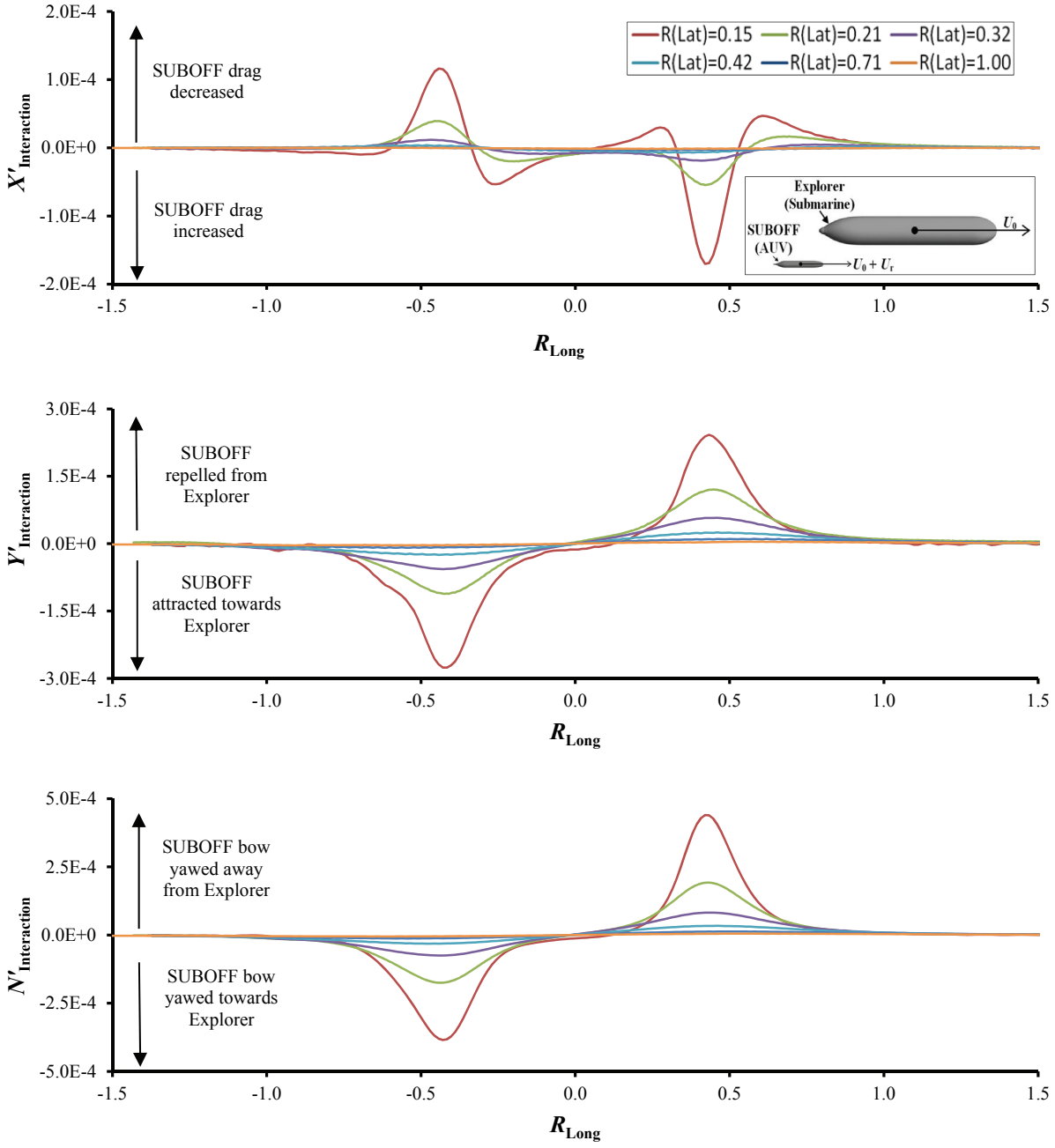

Figure 15: Interaction influence on the SUBOFF's longitudinal force coefficient ($X'_{Interaction}$), lateral force coefficient ($Y'_{Interaction}$), and yawing moment coefficients ($N'_{Interaction}$) vs relative longitudinal position (R_{Long}) for the AUV overtaking the submarine at different R_{Lat}. The forward speeds of the SUBOFF and Explorer are 3.0 m/s and 1.5 m/s respectively (i.e. U_0 = 1.5 m/s, U_r = 1.5 m/s).

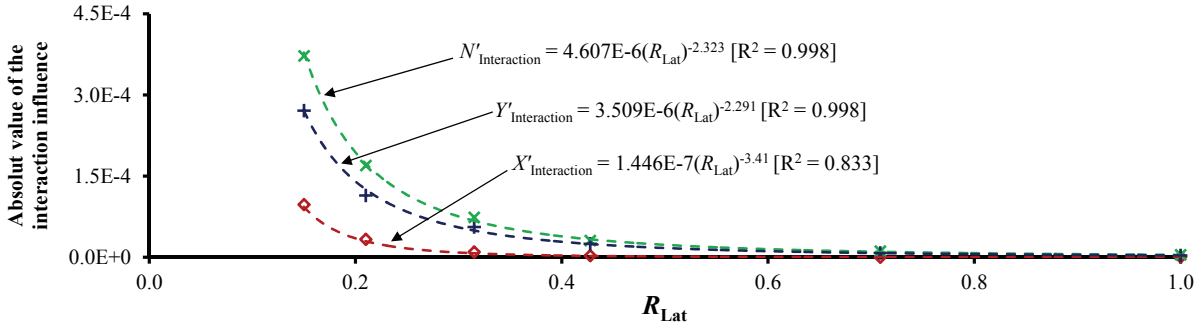

Figure 16: Power regression analysis of the interaction influence on the SUBOFF's longitudinal force coefficient ($X'_{Interaction}$), lateral force coefficient ($Y'_{Interaction}$), and yawing moment coefficients ($N'_{Interaction}$) as a function of R_{Lat} for the AUV overtaking the submarine at the R_{Long} of 0.4. The forward speeds of the SUBOFF and Explorer are 3.0 m/s and 1.5 m/s respectively (i.e. U_0 = 1.5 m/s, U_r = 1.5 m/s).

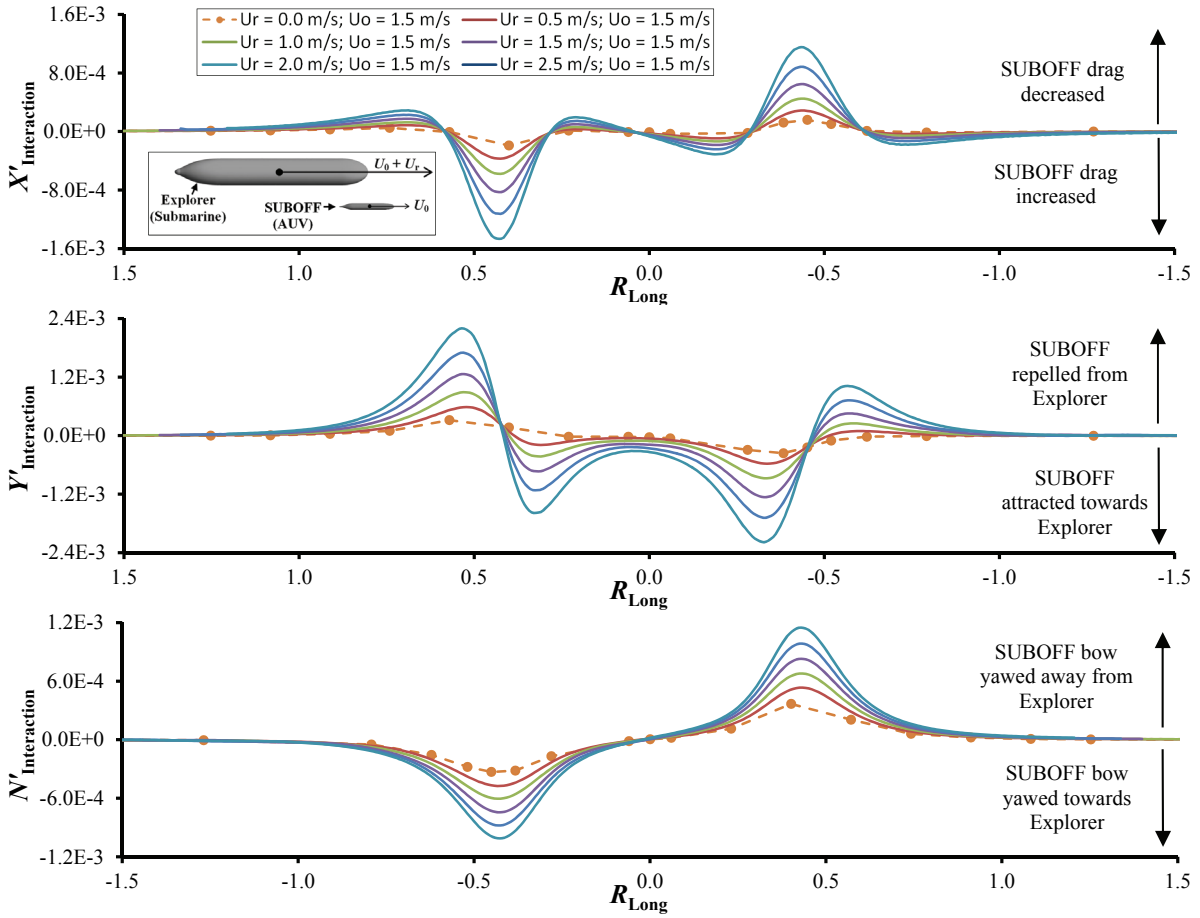

Figure 17: Interaction influence on the SUBOFF's longitudinal force coefficient ($X'_{Interaction}$), lateral force coefficient ($Y'_{Interaction}$), and yawing moment coefficients ($N'_{Interaction}$) vs relative longitudinal position (R_{Long}) for the submarine overtaking the AUV at different relative speeds.